scientific reports

Check for updates

OPEN

# Role of alpha-1 antitrypsin in Bruch's membrane integrity

Shun-Yun Cheng[1], Delaney Giguere[1], Ilana Silverstein[1], Adrienne Conza[1], Johanna M. Seddon[1], San Kim[1], Takeshi Iwata[2], Christian Mueller[3] & Claudio Punzo[1,4,5]✉

**Alpha-1 antitrypsin (AAT) is a serine protease inhibitor that plays a crucial role in maintaining extracellular matrix integrity. Studies suggest that AAT augmentation therapy may benefit multiple eye diseases, including age-related macular degeneration (AMD). However, the function of endogenous AAT in the eye remains unclear. Here we used genetic knockout mice to study the role of AAT in eye health. We show that loss of AAT results in Bruch's membrane (BrM) thickening driven in part by increased laminin deposition with a concomitant decrease in collagen and elastin, which are two other critical BrM components. Interestingly, BrM remodeling due to excess extracellular protease activity reduced the age-related deposition at the BrM of apolipoprotein E, while increasing complement factor H and lowering secretion of the proangiogenic vascular endothelial growth factor. Despite these changes, the phagocytic function of the retinal pigment epithelium was not affected nor was the expression of genes that partake in photoreceptor cell metabolism. Consistent with loss of AAT resulting in changes that should alleviate AMD pathologies, human AMD donor eyes exhibited lower AAT expression levels in the BrM/choroid layer when compared to healthy donor eyes. Together, the study provides insight into AAT's function and its potential involvement in AMD.**

**Keywords** Alpha-1 antitrypsin, Age-related macular degeneration, AAT, A1AT, AMD risk alleles, Bruch's membrane

Alpha-1 antitrypsin (AAT) is an antiprotease that is primarily produced by the liver. It plays a crucial role in modulating the innate immune response in the human body as an acute-phase protein[1]. Disease-related mutations in the *SERPINA1* gene, which encodes for AAT, result in misfolded proteins that accumulate in the liver and are poorly secreted into the bloodstream[2]. AAT inhibits several extracellular matrix (ECM)-degrading enzymes by forming stable complexes with serine proteases such as elastase and collagenase, thereby protecting the ECM from excess protease-mediated damage. In the lungs, dysfunctional or deficient AAT can lead to unchecked neutrophil elastase activity, resulting in progressive tissue damage that leads to conditions such as emphysema and chronic obstructive pulmonary disease (COPD)[3].

As a compensatory treatment, AAT augmentation therapy has demonstrated positive outcomes in slowing the decline of lung function, reducing loss of lung density, and providing long-term benefits for patients with emphysema and COPD resulting from severe AAT deficiency[4]. Beyond treating AAT deficiency, its role in modulating inflammation has garnered interest for potential applications in diseases such as type 1 diabetes, inflammatory bowel disease, and rheumatoid arthritis[5–7]. While predominantly produced by hepatocytes, AAT is also expressed in various other cell types, suggesting it functions across different tissues[1].

In the eye, AAT maintains corneal integrity and transparency and shifts microglia from a pro-inflammatory to an anti-inflammatory state when supplemented[8,9]. A recent study suggested that the mutant PiZ allele of AAT reduces risk for age-related macular degeneration (AMD), while the mutant PiS allele increases risk[10]. Since AAT inhibits elastase and collagenase it is predicted to play a crucial role in the integrity of the Bruch's membrane (BrM). The BrM is an ECM rich in collagen and elastin that is situated between the choriocapillaris and the retinal pigmented epithelium (RPE), keeping RPE cells in place and facilitating nutrient transport from the choroidal vasculature to photoreceptor cells[11]. Disruption of the BrM has been implicated in retinal disease such as AMD[12]. Risk alleles for AMD include many ECM metalloproteases that affect BrM integrity[13–15]. The high temperature requirement serine protease A1 (HTRA1), which cleaves ECM components including elastin and AAT[16], has one of the highest odds ratio for AMD due to a specific single nucleotide polymorphism (SNP)[17]. This specific

[1]Department of Ophthalmology and Visual Sciences, University of Massachusetts Chan Medical School, Worcester, MA 01605, USA. [2]Divivion of Molecular and Cellular Biology, National Institute of Sensory Organ, NHO Tokyo Medical Center, 2-5-1, Higashigaoka, Meguro-ku, Tokyo 152-8902, Japan. [3]Genomic Medicine Unit, Sanofi, Waltham, MA 02451, USA. [4]Department of Genetics and Cellular Medicine and Horae Gene Therapy Center, Worcester, MA 01605, USA. [5]Department of Neurobiology, University of Massachusetts Chan Medical School, Worcester, MA 01605, USA. ✉email: Claudio.Punzo@umassmed.edu

SNP is associated with elevated HTRA1 protein expression levels[17]. However, a recent report proposes that this SNP reduces, rather than increases levels of HTRA1, meaning that reduced levels increase the odds for AMD[18]. In mice, overexpression of HTRA1 leads to BrM changes that exacerbate choroidal neovascularization (CNV), an advanced form of AMD, when mice are exposed to cigarette smoke[19,20]. Interestingly, AAT supplementation mitigates some of the effects of increased HTRA1 expression[21], one of which is increased vascular endothelial growth factor (VEGF) production[21,22]. Consistent with that finding ex vivo sprouting assays from choroidal tissue of HTRA1 overexpressing mice demonstrated an HTRA1-dependent increase in sprouting that is inhibited by AAT[21]. Additionally, AAT supplementation speeds the recovery of CNV lesions in a natural model of CNV as well as in the laser induced model of CNV[21]. AAT has also been proposed to have a proangiogenic role by increasing VEGF in various cells[23–25], and by preventing elastase from inactivating VEGF by cleavage[26].

The data attributes an important role to AAT in maintaining BrM and retinal integrity. However, the role of endogenous AAT remains unclear. To elucidate the role of AAT within the eye we analyzed mice with a genetic loss of AAT that includes the deletion of all five *Serpina1* paralogs[27]. We found that loss of AAT leads to early changes in the BrM that are exacerbated with age, while the RPE and the neural retina are only mildly affected. These changes include a reduction of collagen and elastin in the BrM accompanied by a compensatory increase in laminin. Interestingly, eliminating AAT activity reduces VEGF levels in the retina of young and aged mice and in the RPE of aged mice. Additionally, removal of AAT reduces the age-related accumulation of lipoproteins, and increases complement factor H (CFH) and HTRA1 at the BrM. Since some of these changes are associated with AMD, we analyzed the expression of AAT in tissues from eye donors with and without AMD. We found reduced expression of *SERPINA1* at the RPE/choroid when compared to non-diseased individuals, suggesting that the reduction might be an adaptive response to the disease in patients with AMD.

## Results

### AAT deficient mice develop normal age-dependent fundus pathologies

To elucidate the role of AAT in eye health we utilized a genetic knockout model of the *Serpina1* gene (hereafter referred to as $AAT^{-/-}$ mice)[27]. Retinal health was monitored using funduscopy, fundus fluorescein angiography (FFA), and optical coherence tomography (OCT) at 2 months (2 M) of age and in mice aged between 18 and 24 M. No significant retinal abnormalities were observed in $AAT^{-/-}$ mice by these methods at 2 M of age (data not shown). At 18-24 M of age, both $AAT^{-/-}$ and littermate control ($AAT^{+/+}$) mice exhibited microglia migration in the retina (Fig. 1a, b), a common characteristic observed in aged mouse retinas[28]. One mouse developed geographic atrophy (GA) and CNV (Fig. 1a, b). Collectively, the non-invasive imaging data suggests that loss of AAT function can lead in rare instanced to advanced AMD-like pathologies in mouse; however, overall eye health seem to be minimally affected as assessed by these methodologies.

### Altered Bruch's membrane composition in $AAT^{-/-}$ mice

AAT is predicted to play an important role in BrM integrity. To determine if loss of AAT affects the BrM we performed a more detailed characterization by immunofluorescence and electron microscopy. The BrM consists of five distinct layers: the basement membrane of the RPE, the inner collagenous layer, the elastic layer, the outer collagenous layer, and the basement membrane of the choriocapillaris, which helps maintain retinal health by facilitating nutrient transport from the choroid to the RPE. To investigate whether different ECM layers in the BrM are affected by loss of AAT, three major ECM components, collagen IV (COL IV), laminin, and elastin, were evaluated in $AAT^{-/-}$ retinas at 18-24 M of age using immunofluorescence staining or western blotting analyses (Fig. 2). COL IV, the major ECM component in the collagenous layer showed reduced signal in the BrM of $AAT^{-/-}$ mice at 18-24 M of age compared to age-matched $AAT^{+/+}$ mice (Fig. 2a, c). Similarly, elastin protein levels were reduced in $AAT^{-/-}$ by 40% in protein extracts from the choroid/RPE tissue compared to littermate controls $AAT^{+/+}$ (Fig. 2b). Both, collagenase and elastase are two ECM proteases that are normally inhibited by AAT. Conversely, Laminin gamma 3, known for its role in retinal development[29], showed a higher expression signal in immunofluorescence and approximately a 2.5-fold increase in protein level by western blot analysis (Fig. 2a–c). The increase in Laminin was confirmed with a second antibody specific to the subunits Laminin-1/2 (alpha-1/2, beta-1, and gamma-1) (Fig. 2a, c). To understand how early these changes start to occur, we analyzed the expression of these genes by immunofluorescence on retinal sections of 2 M old mice (Fig. 2d). None of these proteins showed any change by immunofluorescence suggesting that these changes are a consequence of prolonged loss of AAT and that the increase in Laminin expression might reflect a compensatory mechanism to balance the reduction of the other ECM components in the BrM.

To further understand how the different layers of the BrM are affected and confirm changes in BrM thickness, we characterize $AAT^{-/-}$ eyes by electron microscopy (Fig. 3). In aged wildtype mice, we observed BrM thickening (blue arrows), increased lipid deposition (red asterisk), and Elastin fragmentation (yellow asterisks), similar to findings reported by other research groups in aged mice[30] (Fig. 3a, b). These findings were exacerbated in aged $AAT^{-/-}$mice. The BrM was much thicker and more distorted, especially in the basement membrane of the RPE (red double arrow) and the basement membrane of the choriocapillaris (yellow double arrow), consistent with the increased Laminin deposition detected by immunofluorescence and western analysis. It is unclear what the disorganized electron dense fragments in aged mutant mice represent. They appear to be of different lengths suggesting that they could represent fragments of the proteins that are reduced such as Collagen and Elastin, as well as fragments of Laminin, which is increased. Interestingly, although by immunofluorescence the BrM appeared normal at 2 M of age, we observed changes by electron microscopy in $AAT^{-/-}$ mice as early as 3 M of age (3 M), resulting in BrM thickening (blue double arrow) and less organized RPE basal infoldings (Fig. 3c). Together, the data indicate that AAT is constantly required to maintain BrM integrity and that its loss leads to slow adaptive changes over time.

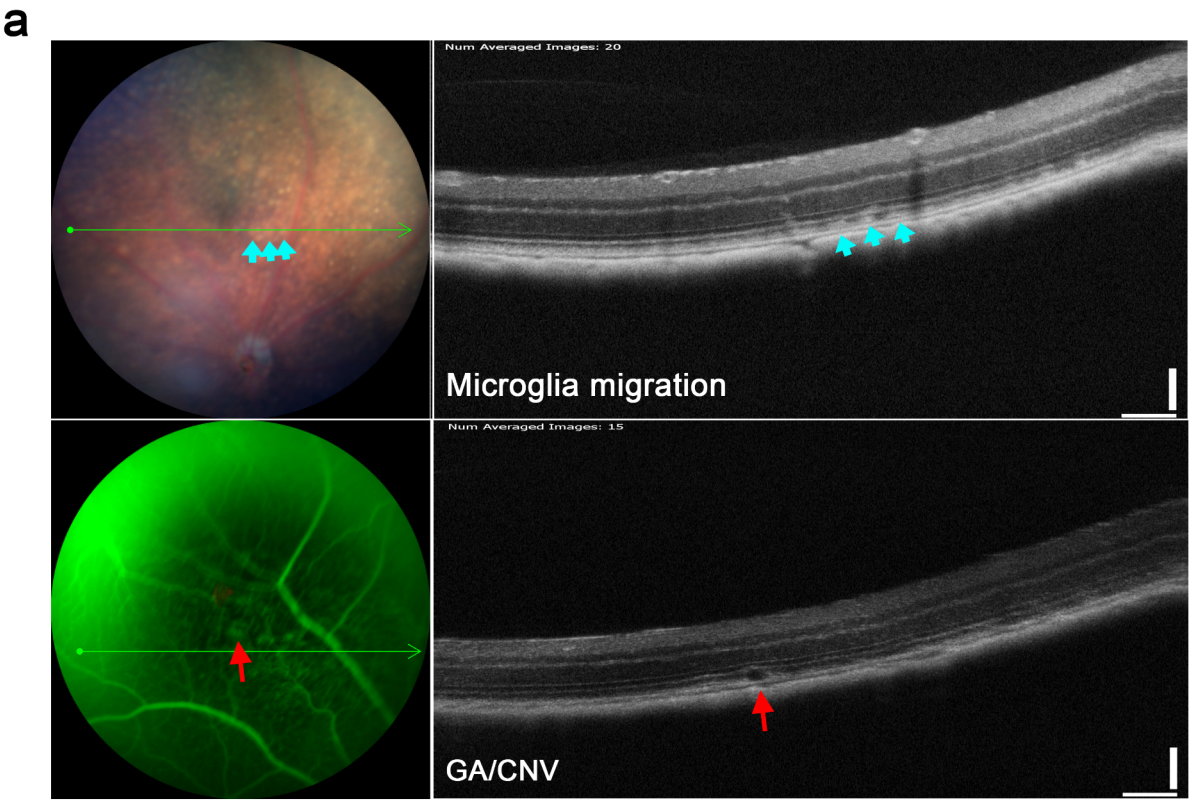


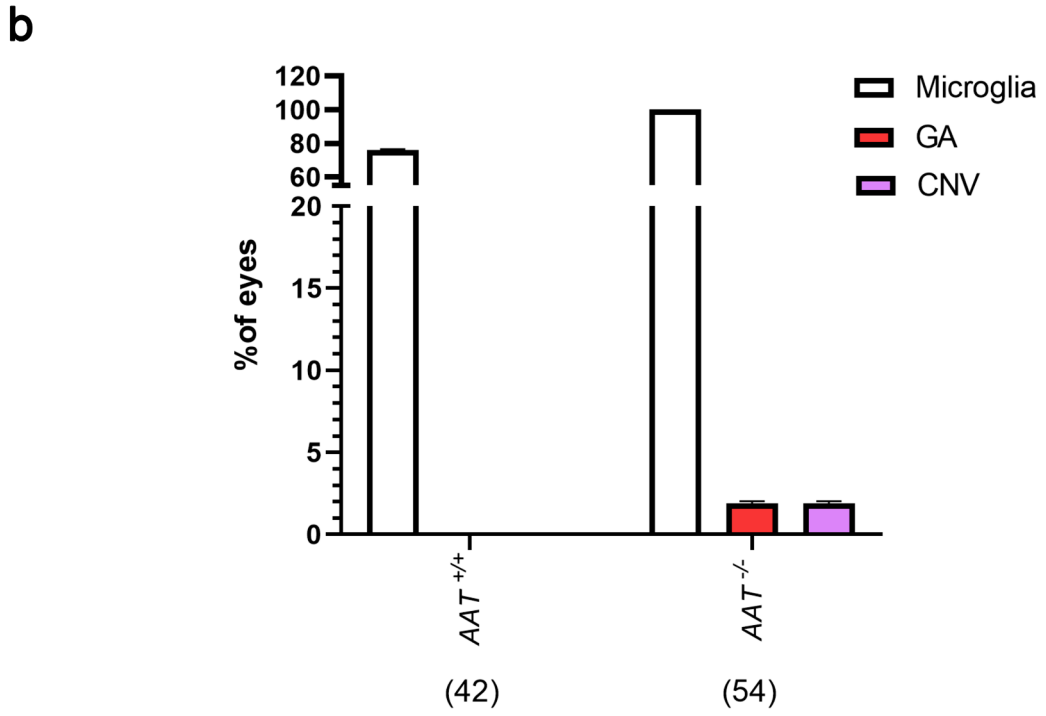


**Fig. 1**. AAT$^{-/-}$ mice exhibited normal age-related pathologies at 18-24 M. (**a**) Fundus images and corresponding OCT scans (green line) show microglia migration (cyan arrows, top panel). In one aged *AAT*$^{-/-}$ mouse (bottom row), the retina developed GA (red arrow) and neovascular pathologies as seen by OCT and FFA, respectively. Scale bar: 100 µm. (**b**) Percentage distribution of microglia and disease phenotypes shown in (a) in *AAT*$^{-/-}$ mice at 18-24 M of age. Bars show percentage ± margin of error (M.O.E.). Numbers in parentheses indicate the number of eyes analyzed.

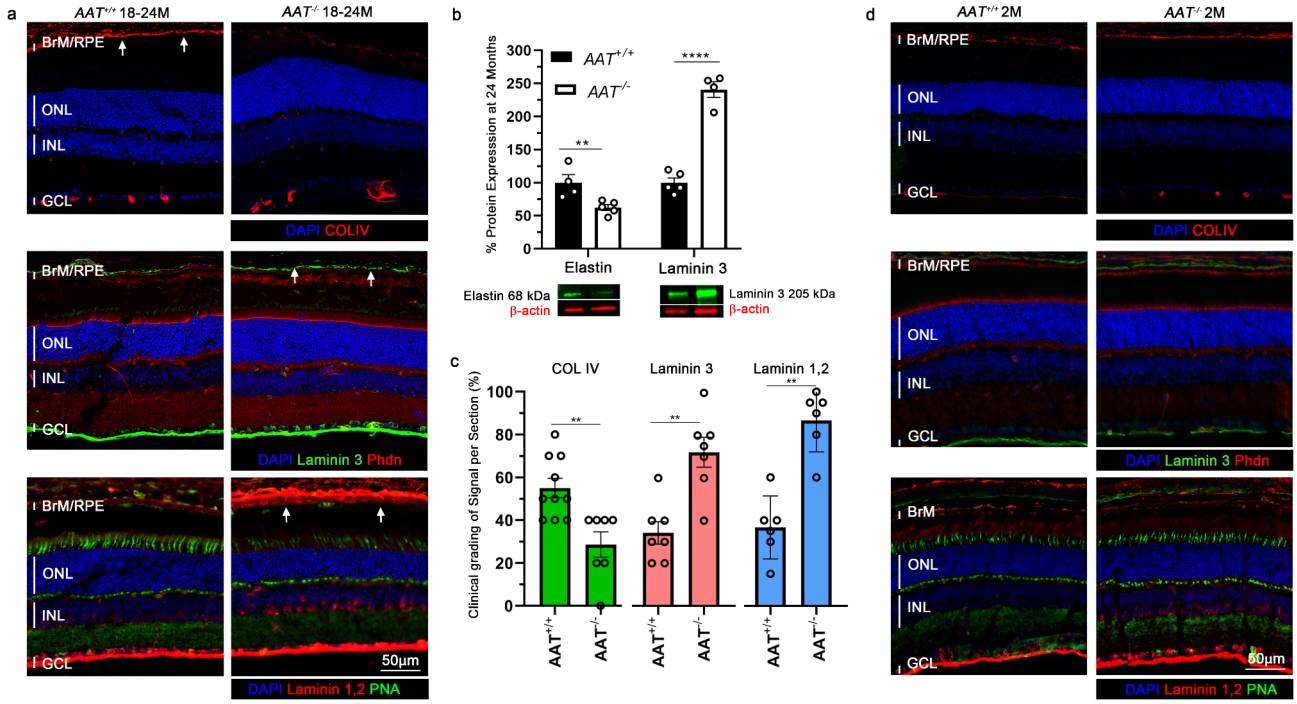


**Fig. 2.** Histological and molecular changes in AAT$^{-/-}$ mice. (**a**) Immunofluorescence on retinal cross sections of 18-24 M old wildtype mice (*AAT*$^{+/+}$, left column) and *AAT*$^{-/-}$ mice (right column). Collagen IV (COL IV, red; first row) shows a reduction in signal at the RPE/BrM, while the laminin 3 (green; second row) and laminin 1,2 (red; third row) signal is increased. Scale bar: 50 µm; Blue: nuclear DAPI; red: Phalloidin in second row marking RPE cells; green: PNA in third row marking photoreceptor cells; BrM/RPE: Bruch's membrane and retinal-pigmented epithelium layers; ONL, outer nuclear layer; INL, inner nuclear layer; GCL, ganglion cell layer; vertical lines mark thickness of layers indicated; white arrows mark RPE/BrM region. (**b**) Western blot analysis with RPE/choroid protein extracts from 18-24 M old mice of genotypes indicated. Elastin levels are reduced while Laminin 3 levels are increased in *AAT*$^{-/-}$ mice, confirming the histological findings in (**a**). Examples of western blot bands are shown beneath the bar graph. Bars show percentage protein ± S.E.M.; $N = 4–5$ mice; $^{**}p < 0.01$; $^{****}p < 0.0001$. (**c**) Clinical grading of histological immunofluorescence stainings shown in panel (**a**) with mice 18-24 M of age. Antibody staining for the proteins in question was analyzed across the entire section and a percentage number was assigned as to the uniform covered length of the signal across the entire section. Each dot represents the eye of 1 animal. (**d**) Immunofluorescence on retinal cross sections of 2 M old wildtype mice (*AAT*$^{+/+}$, left column) and *AAT*$^{-/-}$ mice (right column). Same antibodies and labeling were used as shown in panel (**a**), with no obvious change in expression seen at the RPE/BrM for all these proteins.

## Loss of AAT does not affect RPE phagocytosis and photoreceptor metabolism

Loss of AAT altered RPE cell structure, especially the basal infoldings. The RPE basal infoldings are finger-like extensions from the basal surface of the RPE cell towards the BrM that increase the surface area of the cell thereby enhancing nutrient transport from the fenestrated choroidal vasculature. Furthermore, they provide structural stability by anchoring the cells to the BrM. In both young and aged *AAT*$^{-/-}$ mice, RPE basal infoldings were thinner and more deformed, resulting in less connectivity to the BrM (Fig. 3b, c). Notably, basal infoldings are already affected by 3 M of age (Fig. 3c). To investigate whether these changes in cellular morphology affect RPE cell function we monitored the digestion of photoreceptor outer segments (POS). Studies have shown that POS shedding is regulated by circadian rhythms, and dysregulation in the digestion of POS, can contribute to disease pathologies such as AMD[31]. We did not find any significant difference in POS shedding and digestion between *AAT*$^{-/-}$ mice and littermate control mice at 10 M of age suggesting that RPE function is not compromised in *AAT*$^{-/-}$ mice (Fig. 4a, b). The age was chosen as a halfway point between young and aged mice in order to avoid all the microglia that are seen in very old mice but to have mice that are old enough to see if a difference is detectable.

Altered RPE basal infoldings and thickened BrM could affect the neural retina by changes in nutrient transport from the choroidal vasculature to photoreceptor cells. Previous studies showed that photoreceptor cells adapt to nutrient shortage by increased activity in mTORC1 and increased expression in glycolytic genes to promote photoreceptor cell survival[31–33]. To assess photoreceptor cell survival, we measured the thickness of the outer nuclear layer (ONL). At 18-24 M, no difference in ONL thickness was seen between *AAT*$^{-/-}$ mice and *AAT*$^{+/+}$ littermates (Fig. 4c). To assess photoreceptor cell metabolism, we performed western blot analyses for phosphorylated ribosomal protein S6 (pS6), a bona fide readout for mTORC1 activity, in addition to Hexokinase-2 (HK2) and Pyruvate kinase muscle isoenzyme M2 (PKM2). We found a 3.5-fold increase of

pS6 protein levels in aged $AAT^{-/-}$ retinal extracts, while HK2 and PKM2 protein levels remained unchanged between $AAT^{-/-}$ and $AAT^{+/+}$ littermates (Fig. 4d). To determine if the changes in pS6 levels were due to increased phosphorylation of S6 in photoreceptor cells we performed an immunofluorescence analysis, which showed an increase in the inner nuclear layer reminiscent of a Müller glia cell pattern (Fig. 4e). While the significance of this increase in Müller glia cells remains unclear it appears to be age dependent as it was not seen in young $AAT^{-/-}$ mice at 2 M (Fig. 4e). Together, the data suggest that while the overall homeostasis of the neural retina may be affected with age, photoreceptor cells seem to not suffer from an overt shortage of nutrient supply.

## Effects of AAT loss on AMD-related proteins

We previously showed that there is an age-dependent increase in lipoprotein and complement factor H (CFH) accumulation at the BrM across the mouse eye[31]. Given that BrM thickening, lipoprotein and CFH deposition are associated with AMD[34], we interrogated whether such accumulations remain or are altered with the BrM changes seen in $AAT^{-/-}$ mice. Interestingly, a less uniform accumulation of apolipoprotein E (ApoE) was seen at the BrM and a significant reduction in ApoE protein level was observed in RPE/choroid tissue extracts from aged $AAT^{-/-}$ mice (Fig. 5a). In contrast, CFH accumulation was increased at the BrM of aged $AAT^{-/-}$ mice by immunofluorescence and western blot analysis (Fig. 5b). Since CFH plays a part in the inhibition of the complement cascade[29], this increase might reflect an adaptive response to protect RPE cells from extracellular conditions that might affect RPE survival. Neither ApoE nor CFH showed any difference in signal intensity in young $AAT^{-/-}$ mice when compared to $AAT^{+/+}$ mice (Fig. 5a, b).

The serine protease HTRA1, which can cleave AAT[16] has one of the highest odds ratio for AMD[17]. Since there are contradictory reports on whether increased[17] or decrease[18] expression levels of HTRA1 contribute to AMD we investigated HTRA1 expression in aged $AAT^{-/-}$ mice. We found increased HTRA1 signal in the RPE of $AAT^{-/-}$ mice (Fig. 5c), suggesting that the protein is either stabilized in the absence of AAT or the expression is increased as a compensatory mechanism to modulate the ECM that has changed in composition due to the lack of AAT.

## Loss of AAT reduces VEGF levels

RPE cells are a major source of VEGF in the eye[35]. Reducing VEGF levels in the retina has been shown to have a beneficial effect for AMD patients with CNV[36]. AAT supplementation appears to mitigate some of the effects of increased HTRA1 expression[21], one of which is increased VEGF expression[21,22]. Supplementation of ATT speeds also the recovery of CNV lesions in the laser induced model of CNV[21]. Contrarily, AAT has a proangiogenic role by increasing VEGF in various cells[23–25], and by preventing elastase to inactivate VEGF by cleavage[26]. To see if VEGF levels are affected by loss of AAT, we measured VEGF protein levels from retinal and RPE/choroid extracts by ELISA. We found a significant reduction in the retina and RPE in aged $AAT^{-/-}$ mice (18-24 M). However, in young mice (2 M), only the retinas showed a significant reduction compared to littermate controls (Fig. 6a). To determine if this reduction is biologically relevant, we used the laser-induced model of CNV and evaluated the CNV recovery rate over time. $AAT^{-/-}$ mice showed a better recovery from laser-induced CNV, with 39% of the initial lesions remaining at 20 days (D20) after CNV induction, while the littermate control group had 51% of the initial lesions remaining at D20 (Fig. 6b). The data suggest that AAT levels can alter VEGF expression and modulate neovascularization in the retina.

## AAT expression is reduced at the BrM/choroid of AMD patients

The mouse data suggests that loss of AAT leads to phenotypes that are also seen in AMD patients such as thickened BrM and disorganization of basal infoldings, while alleviating other phenotypes typical of AMD such as ApoE accumulation and VEGF secretion. To better understand the role of AAT in AMD, we examined AAT expression by immunohistochemistry in donor eyes of diseased and non-diseased individuals (Fig. 7). In 3 out of 3 donor eyes diagnosed with either the advanced dry (1 eye) or the neovascular form (2 eyes) of AMD, we detected a lower AAT signal in the BrM/choroid region when compared to age-matched non-diseased donor eyes across the entire section (Fig. 7a, yellow arrows). Since AAT is a secreted protein that is mainly produced by hepatocytes the reduction of AAT at the BrM/Choroid could be either due to lower AAT serum levels or reduced local production in the eye. To determine if there are local adaptations, we examined the local synthesis of the *SERPINA1* gene using RNAscope to visualize mRNA expression. Both, non-diseased and diseased eyes exhibited similar expression patterns in the neural retina. However, in the choroid, *SERPINA1* expressing cells were only detected in non-diseased eyes (Fig. 7b, yellow arrows), suggesting that there is a disease specific adaptation to down-regulate the local expression of AAT in AMD.

# Discussion

AAT is a serine protease inhibitor that functions in different tissues to maintain homeostasis. Here, we showed that endogenous AAT plays a crucial role in maintaining the integrity of the BrM. The disruption of the BrM, marked by a reduction in collagen and elastin is likely due to uncontrolled collagenase and elastase activity over time. Interestingly, this protease-antiprotease imbalance results in a compensatory mechanism that leads to increased laminin deposition in the BrM. Surprisingly, RPE phagocytosis remains unaffected although these BrM changes lead to deformed RPE basal infoldings and loosening connections with the BrM. These changes appear to not affect the transfer of nutrients from the choriocapillaris to photoreceptor cells as key glycolytic genes showed no difference in expression. Consistent with this finding there was no obvious photoreceptor cell degeneration in $AAT^{-/-}$ mice. The reason for the increase in S6 phosphorylation (pS6) in the inner nuclear layer remains unclear. Further studies are needed to fully understand the effects of AAT loss on ocular health and how these changes contribute to AMD.

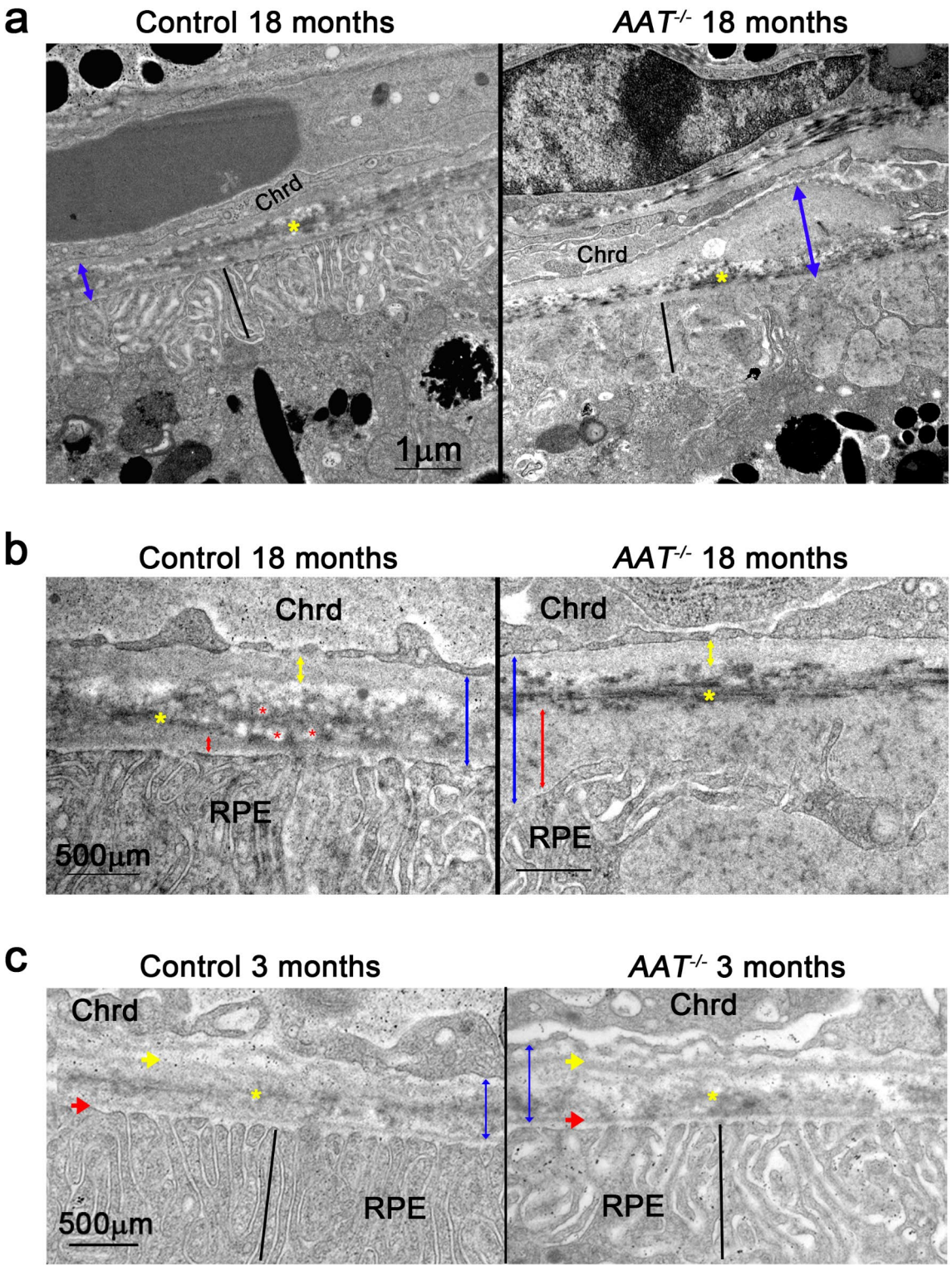


AAT facilitates anti-inflammatory responses and maintains ECM integrity, making it an ideal therapeutic target for retinal diseases such as AMD. In AMD donor eyes, we detected lower level of AAT in the BrM/choroid layer, and no mRNA synthesis in the choroid. This suggests that there are disease-associated changes in AAT expression levels. Supplementation may provide beneficial effects in the disease development. Conversely, the local downregulation of AAT may reflect an adaptive response to protect the tissue from further damage. AAT has proangiogenic[23–25] as well as anti-angiogenic effects[21,22] depending on the cell type and circumstances[37,38]. This may be related to a protease-antiprotease imbalance that affects the ECM of blood vessels[38]. Depending on the tissue and blood vessel type there may be different responses with regards to VEGF levels. We found that *AAT*$^{-/-}$ mice exhibited lower expression of VEGFA in both retina and RPE tissue, and a faster recovery rate from laser-induced CNV, while others have shown that AAT supplementation speeds recovery of CNV lesions in a

◀**Fig. 3**. Changes by EM in young and aged AAT$^{-/-}$ mice. (**a**) Electron microscopy (EM) images of 18 M old mice showing BrM thickening and changes in RPE basal infoldings in littermate control (*AAT*$^{+/+}$; left column) and *AAT*$^{-/-}$ mice (right column). Size of BrM is indicated by blue double arrows. Basal infoldings of the RPE are marked by black line. They are significantly disorganized in the *AAT*$^{-/-}$ mice. The elastin layer is marked by a yellow asterisk. (**b**) Higher magnifications of same genotypes and ages as shown in (**a**) showing the basement membrane of the choriocapillaris (yellow double arrow) and of the RPE (red double arrows). Lipid droplets are also seen particularly in wild-type littermate control mice (red asterisk). (**c**) EM images of young 3 M old mice showing early BrM changes including a thicker BrM (blue double arrow). Basal infoldings are less organized in *AAT*$^{-/-}$ mice (black line). Chrd, choroid; RPE, retinal-pigmented epithelium; blue double arrows: thickness of BrM; yellow arrows or double arrows: basement membrane of the choriocapillaris; red arrows or double arrows: basement membrane of the RPE; yellow asterisk: elastin layer; red asterisk: lipid droplets; black lines: basal infoldings of RPE cells).

natural model of CNV as well as in the laser induced model of CNV[21]. Thus, it remains unclear which strategy might be more beneficial to treat a disease like AMD, augmentation or silencing of AAT.

The *SERPINA1* gene has been suggested to be associated with AMD increasing or decreasing disease risk depending on the mutant allele[10]. Many AMD risk genes are ECM proteases or protease inhibitors[14,15,39,40], with HTRA1 being the protease with the highest odds ratio[17]. Interestingly, smoking is the biggest environmental risk factor for AMD[41,42]. Coincidently, cigarette smoke in the lungs can inactivate AAT's inhibitory function[43]. Thus, it is possible that smoking as an environmental risk factor contributes to AMD risk via reduction of serum AAT and thus via a protease-antiprotease imbalance rather than direct oxidation of RPE cells. Consistent with this idea, the disruption of BrM and RPE integrity in *AAT*$^{-/-}$ mice resembles that in mice exposed to chronic cigarette smoke[44]. Additionally, loss of AAT increased HTRA1 expression in the RPE. Given the role ECM proteases play in maintaining BrM integrity, and the role the BrM plays in RPE and retinal health, it is not surprising that a protease-antiprotease imbalance changes the AMD disease risk. However, considering our findings that loss of AAT reduces ApoE accumulation at the BrM, which is an accepted hallmark of disease progression and a component of drusen[34], and increases CFH deposition at the BrM, which is a protective mechanism against advanced AMD[45], one could argue that reduction of AAT should reduce disease risk.

The human tissue samples that we analyzed showed a local reduction in AAT that can be interpreted as a protective adaptive response of the tissue. Therefore, depending on the type of protease-antiprotease imbalance, AMD disease risk may increase or decrease. In this regard the findings on the effect of HTRA1 protein levels remain contradictory[17,18]. All these findings open the intriguing possibility that AMD risk genes fall into two distinct categories: risk genes that are directly involved in the pathobiology of the disease, such as genes involved in lipid metabolism, and risk genes that happen to affect the same tissue and cells that are affected in AMD, such as ECM modulating genes, but are otherwise unrelated to the pathobiology of the disease. In that regard we found one rare instance of a mouse progressing to advanced AMD-like phenotypes including RPE atrophy and neovascular pathologies although *AAT*$^{-/-}$mice did not otherwise display classical hallmarks of early AMD, such as lipid accumulation at the BrM. Individuals who develop early AMD and have risk genes that result in a protease-antiprotease imbalance may thus be caught in the crossfire between a natural disease progression and an independent insult that affects the same area. This may complicate the development of precision medicine approaches that target risk genes, since therapeutic effects may be limited for risk genes that are not part of the pathobiology. In conclusion, this study is the first to report the effects of AAT loss in the eye, shedding light on the crucial role of endogenous AAT in maintaining the health of the outer retina, particularly the BrM and RPE.

## Materials and methods

### Animals

All procedures involving animals were in compliance with the Association for Research in Vision and Ophthalmology Statement for the Use of Animals in Ophthalmic and Vision Research. All animal work was approved by the Institutional Animal Care and Use Committees (IACUC) of the University of Massachusetts Chan Medical School. Euthanasia of mice was performed by asphyxiation. Anesthesia was performed by Ketamine/Xylazine. Both, euthanasia and anesthesia were performed according to the guidelines of the American Veterinary Medical Association (AVMA) for mouse euthanasia and anesthesia. The DEA license for the use of ketamine is in Dr. Claudio Punzo's name. The use of the laser for the laser induced choroidal neovascular mouse model was approved by the Radiation Safety Office and the IACUC of the University of Massachusetts Chan Medical School. All users underwent specialized training for the use of the laser. The *AAT*$^{-/-}$ mice used in this study were provided by Dr. Christian Mueller. Generation of the mice has been described in the original publication[27]. HTRA1 overexpressing mice were provided by Dr. Takeshi Iwata and described in their original publication[20]. All animal experiment were in accordance with the ARRIVE Guidelines for the reporting of animal experiments. The ages of the mice used ranged from 2 M to 24 M as indicated in the figures. All mice were genotyped for the absence of the retinal degeneration 8 (*rd8*) allele, which harbors a mutation in the Crumbs 1 gene[46].

### Human donor eyes

Donor tissues were obtained from the Eye Donation Project under the protocol of JMS that was approved by the Institutional Review Board (IRB) of the University of Massachusetts Chan Medical School. Informed consent was obtained from all donors. The study adhered to relevant ethical standards and guidelines. Human retinal tissues were obtained from patient donors with and without AMD who participated in our eye donation

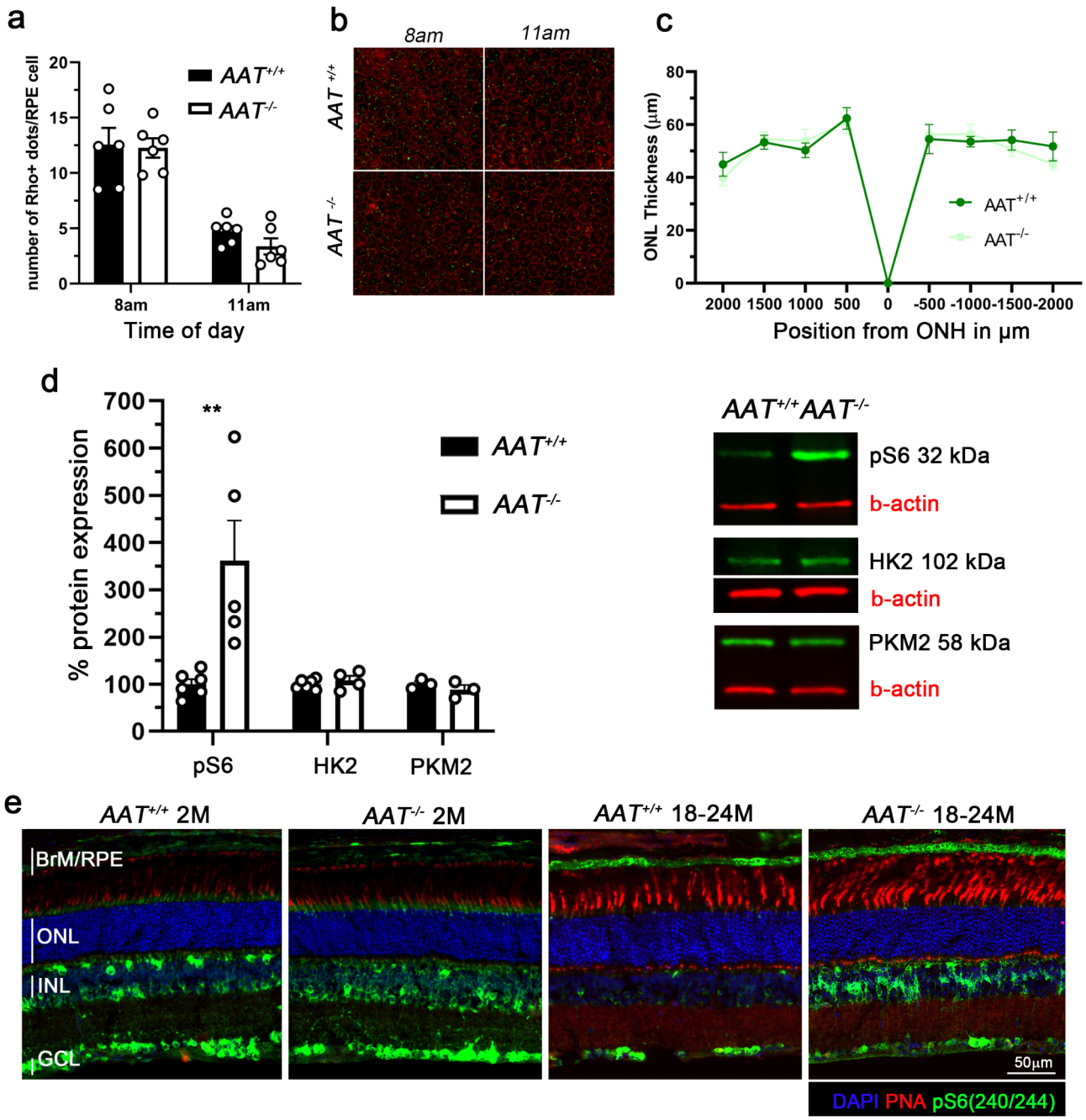


**Fig. 4**. Retinal homeostasis in aged AAT$^{-/-}$ mice. (**a**) Quantification of photoreceptor outer segment clearance at 8am and 11am in littermate control (black bars) and *AAT*$^{-/-}$ mice (white bars) showing no significant difference in the clearance of outer segments at 10 M of age ($N = 6$). (**b**) Representative images used for the quantification. (**c**) Measurements of outer nuclear layer (ONL) thickness at 18-24 M in *AAT*$^{+/+}$ mice (dark green) and *AAT*$^{-/-}$ mice (light green). Each symbol represents the mean ± S.E.M from $N = 5$ retinas. Y-axis shows the thickness in microns and X-axis shows the distance from the optic nerve head (ONH) in µm. (**d**) Western blot analysis for pS6, HK2 and PKM2 expression levels with retinal protein extracts from *AAT*$^{-/-}$ mice (white bars) and *AAT*$^{+/+}$ mice (black bars) at 18-24 M. Bars show percentage expression ± S.E.M.; $N = 5$–6 mice; $^{**}p < 0.01$. Examples of western blot bands are shown to the right of the bar graph. (**e**) Immunofluorescence staining for pS6 (green) on retinal cross sections of *AAT*$^{+/+}$ (first and third image) and *AAT*$^{-/-}$ mice (second and fourth image) at 2 M and 18-24 M. Scale bar: 50 µm; Blue: nuclear DAPI; red: PNA to visualize cone segment; BrM/RPE: Bruch's membrane and retinal-pigmented epithelium layers; ONL, outer nuclear layer; INL, inner nuclear layer; GCL, ganglion cell layer, vertical lines mark thickness of layers indicated.

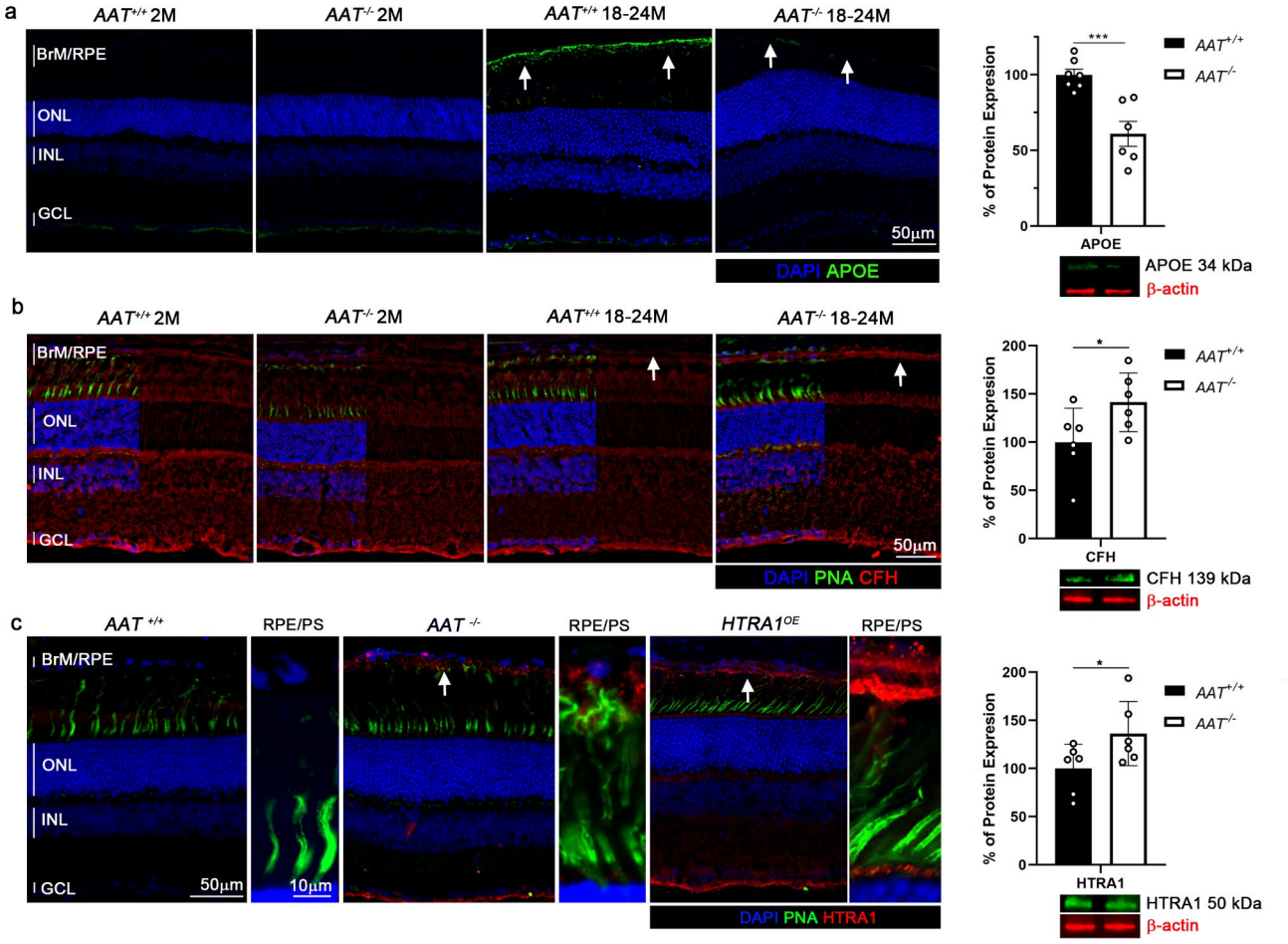


**Fig. 5**. ApoE, CFH, and HTRA1 protein levels in $AAT^{-/-}$ mice. (**a**) Immunofluorescence on retinal cross sections of 2 M old (first and second column) and 18-24 M old mice (third and fourth column) comparing $AAT^{+/+}$ (first and third column) to $AAT^{-/-}$ littermates (second and fourth column). Apolipoprotein E (ApoE; green) displays no signal at the BrM/RPE in 2 M old mice but shows a much stronger signal at the BrM/RPE in aged wildtype mice (white arrows) compared to the aged $AAT^{-/-}$ mice. To the right is a western blot analysis of ApoE protein levels with RPE/choroid tissue extracts from $AAT^{+/+}$ (black bar) and $AAT^{-/-}$ mice (white bar) at 18-24 M to quantify the changes in protein levels seen by antibody staining on sections. Example of western blot bands are shown beneath the bar graph. (**b**) Immunofluorescence on retinal cross sections and western blot analysis following the same format as shown in panel (**a**) for complement factor H (CFH; red) showing an increase in signal at the BrM/RPE (white arrow) of the aged $AAT^{-/-}$ mice compared to the littermate controls or 2 M old mice of either genotype. (**c**) Immunofluorescence on retinal cross sections and western blot analysis of aged (18-24M) $AAT^{+/+}$ and $AAT^{-/-}$ following a similar format as shown in (**a**). Expression of HTRA1 is increased (white arrows) at the BrM/RPE. HTRA1 overexpressing mice ($HTRA1^{OE}$, last panel) were used as a positive control for the HTRA1 antibody staining showing the overexpressed HTRA1 protein at the BrM/RPE region. Next to each panel is a higher magnification of the RPE and photoreceptor outer segment region (RPE/PS; Scale bar: 10 µm). Western blot analysis with RPE/choroid tissue extracts from $AAT^{+/+}$ (black bar) and $AAT^{-/-}$ mice at 18-24 M of age confirming the changes seen by immunofluorescence is to the right. (**a**–**c**) All western blots used 6–7 retinas and stainings were confirmed in at least 3 different biological samples. Bars show percentage expression ± S.E.M.; *$p<0.05$; ***$p<0.001$ Scale bar: 50 µm except for high magnification where it is 10 µm; Blue: nuclear DAPI; green: ApoE in (**a**) and PNA to visualize cone segments in (**b**, **c**); red: CFH in (**b**) and HTRA1 in (**c**); BrM/RPE, Bruch's membrane and retinal-pigmented epithelium layers; ONL, outer nuclear layer; INL, inner nuclear layer; GCL, ganglion cell layer, vertical lines mark thickness of layers indicated.

program[47]. The clinical diagnosis and severity of AMD were determined by ocular examinations and multi-model imaging of the donors in the Seddon Longitudinal Cohort by J.M.S. With the exception of Dr. Seddon, all other authors were not privy to any patient data except age, gender and disease stage. Immunohistochemistry analysis was performed on 20 µm thick retinal cryo-sections of six human donor eyes (age, severity of AMD and gender are indicated in the figures). Three eyes had no clinical evidence of AMD, while three eyes had either geographic atrophy (Grade 4) or CNV (Grade 5B)[48]. Time between death to enucleation ranged from 2 to 9 h.

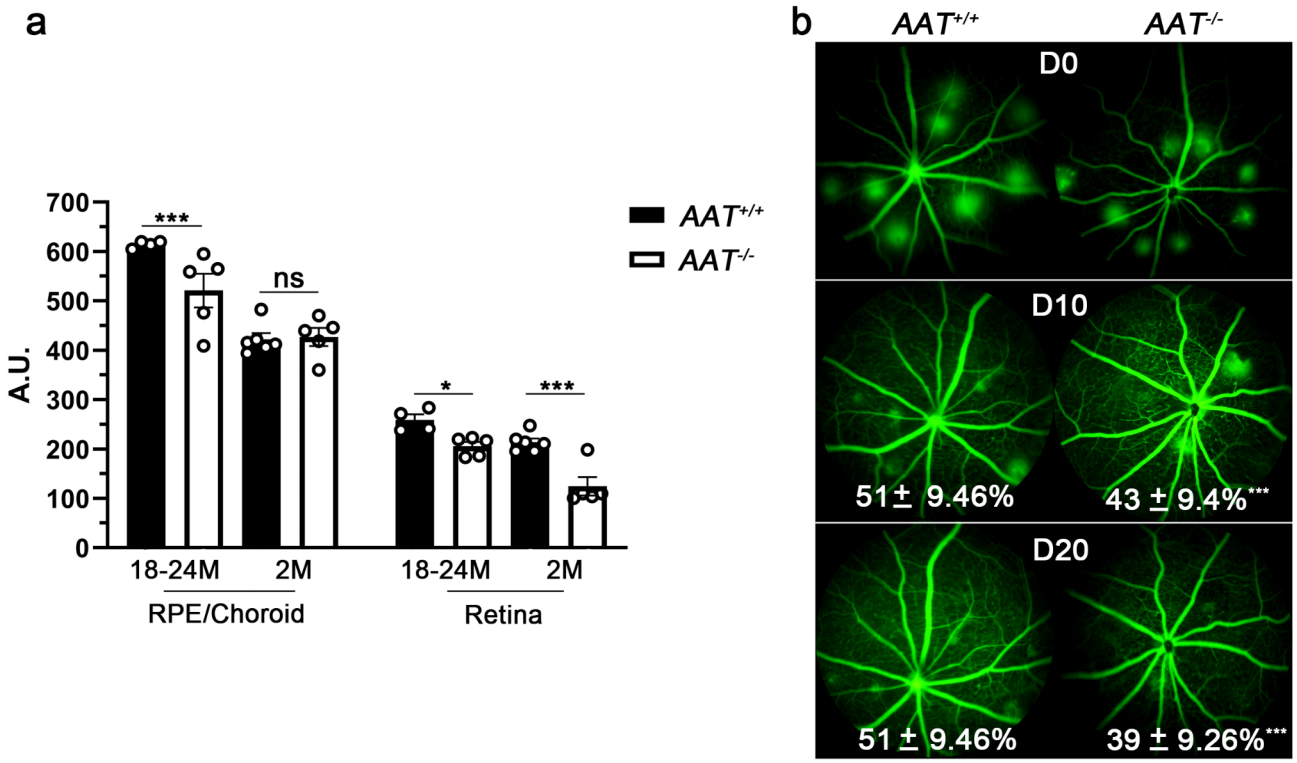


**Fig. 6**. VEGF levels are decreased in $AAT^{-/-}$ mice. (**a**) ELISA with retinal and RPE/choroid extracts probing for VEGF levels in aged (18-24 M) and young (2M) $AAT^{+/+}$ mice (black bars) and $AAT^{-/-}$ mice (white bars). Y-axis shows arbitrary unit (A.U.) ± S.E.M.; $N = 5–6$ mice; $^{*}p < 0.05$, $^{***}p < 0.001$; ns: not significant. (**b**) Recovery from laser-induced CNV showing the percentage of remaining lesions at 10- and 20-days (D: days) post laser damage in $AAT^{+/+}$ mice and $AAT^{-/-}$ mice. The percentage is shown in examples of FFA images ± margin of error (M.O.E.). Number of initial lesions at D0 for $AAT^{+/+}$ mice and $AAT^{-/-}$ mice was 75.

## Laboratory experiments

All laboratory experiments that require biosafety review were approved by the Institutional Biosafety Committee of the University of Massachusetts Chan Medical School.

## Funduscopy, fluorescein angiography (FFA), optical coherence tomography (OCT), and laser-induced CNV

Fundus imaging, FFA, OCT, and laser-induced CNV procedures were performed as previously described[31,49]. Age and number of mice analyzed for each experiment are indicated in figures and/or legends. In brief, mice were anesthetized by an intraperitoneal injection of a ketamine/xylazine (100 mg/kg and 10 mg/kg) mixture. One drop of each, Phenylephrine (2.5%) and Tropicamide (1%) was applied for pupil dilation 10 min prior to the procedure. Animals were kept on a warming plate during the entire time of the procedures to maintain the body temperature at 37 °C. Funduscopy was performed as described[49] utilizing the Micron IV camera (Phoenix Research Labs, Pleasanto, CA, USA). Fundus Fluoresceine Angiography was performed immediately following funduscopy imaging by injecting 125 mg/kg of a fluorescein sodium solution subcutaneously behind the neck. Images were acquired with the Micron IV camera. Laser-induced CNV was performed with the TX-System from IRIDEX (532 nm laser) using the following settings: 100 µm diameter, 100mW power, and a duration of 10ms as previously described[50]. Each mouse eye received 6–8 laser burns distributed across the retina. Fundus imaging and FFA were performed every 10 days after laser damage to track the recovery of lesion sites, as indicated in the figure.

## Histology

Immunohistochemistry (IHC) and immunofluorescence (IF) on cryo-preserved sections (12 µm thickness) and RPE/choroid whole mounts were performed as described previously[31]. The following primary antibodies were used: rabbit anti-PKM2 (1:1000; Cell Signaling Technology, Cat#4053), rabbit anti-COL IV (1:300; Bio-Rad, Cat#2150 – 1470), rabbit anti-HK2 (1:300; Cell Signaling Technology, Cat#2867), rabbit anti-ZO1 (1:100; Invitrogen, Cat#40-2200), mouse anti-Rhodopsin (1:100, Abcam, cat#5417), rabbit anti-laminin 1,2 (1:300; NOVUS, Cat#NB300-144), rabbit anti-laminin 3 (1:300; Abcam, Cat#ab11575) and rabbit anti-HTRA1 (1:300, Proteintech, Cat#55011-1-AP). All primary antibodies were diluted in PBS with 0.3% Triton X-100 and 5% bovine serum albumin (BSA, Cell Signaling Technology). For the rabbit anti-pS6 (Ser240/244) antibody (1:300; Cell Signaling Technology, Cat#5364), PBS was replaced with TBS. For the goat anti-Apolipoprotein E

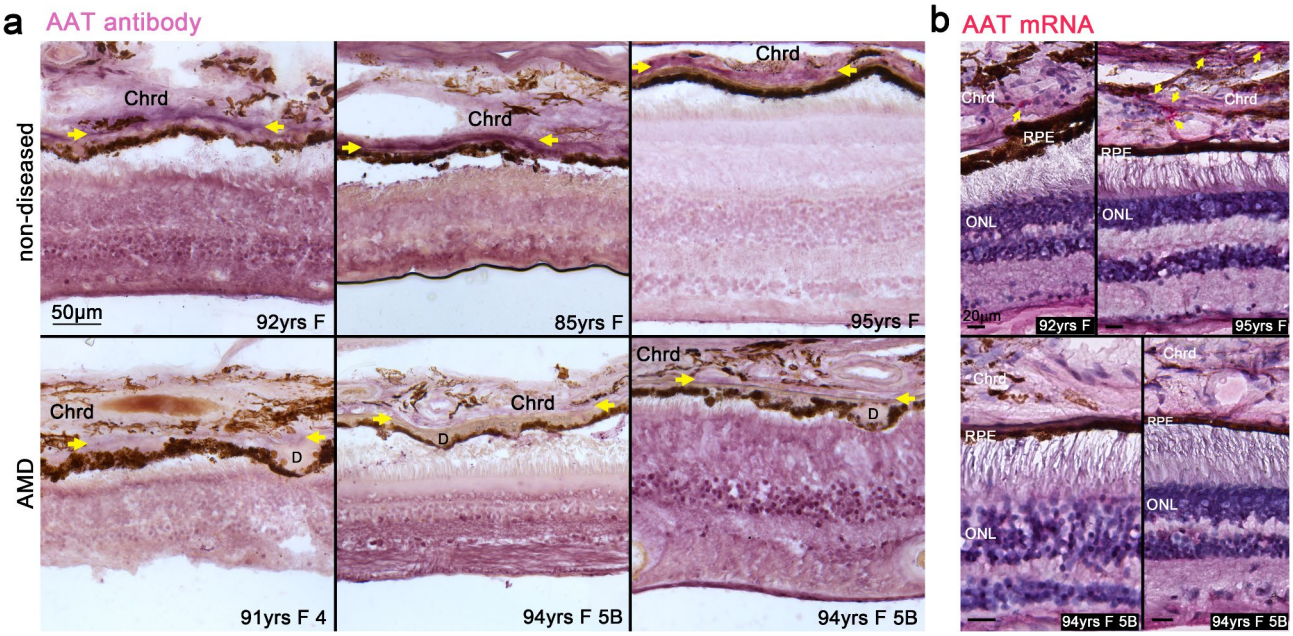


**Fig. 7**. AMD patients exhibit lower AAT expression levels in the choroid. (**a**) Immunohistochemistry (IHC) showing decreased AAT protein levels in the BrM/Choroid layer (yellow arrows) in donor eyes of both, GA (Grade 4) and CNV (Grade 5B) patients (bottom row) when compared to age-matched non-diseased donor retinas (top row; Scale bar: 50 µm; ). Sections from three different donors per group were analyzed. (**b**) AAT mRNA expression (red dotted signal: yellow arrows) is detected in the choroid by RNAscope in non-diseased donor eyes (top; Scale bar: 20 µm), while no signal is seen in AMD patients. Two of the three patients shown in (**a**) are shown in (**b**). Age in years, gender of donor eyes, and disease stage where applicable, is indicated in each panel (Chrd, choroid; ONL, outer nuclear layer; yrs: years; F: female).

(ApoE) (1:1,000, Millipore, Cat#178479) and rabbit anti-complement factor H (1:300; Antibodies Online Cat# ABIN3023097) Triton X-100 was replaced with 0.2% Saponin. The following reagents already had a chromophore conjugated: rhodamine phalloidin (1:1,000; Life Technologies, Cat#R415) and fluorescein peanut agglutinin lectin (PNA) (1:1,000; Vector Laboratories, Cat#FL1071). Nuclei were counterstained with 4′, 6-diamidino-2-phenylindole (DAPI) (Sigma-Aldrich, Cat# 9542). All secondary antibodies (1:1000) were purchased from Jackson Immuno Research and were purified F(ab)2 fragments that displayed minimal cross-reactivity with other species and were all raised in donkey. An exception of this was the immunohistochemistry staining in Fig. 7, which used the ImmPACT VIP kit (Vector Laboratories, Cat# SK-4605). Expression changes were confirmed in at least 3 individual animals per genotype. All images were visualized with a Leica DM6 Thunder microscope with a 16-bit monochrome camera.

## RNA scope

To detect the human *Serpina1* transcripts we used a RNAscope probe from Advanced Cell Diagnostics (Hs-SERPINA1: #435441) according to the manufacturer's instructions. The same cryopreserved sections used for antibody staining were used for this procedure.

## Outer nuclear layer thickness measurement

Quantification of rod survival was performed as previously described[51]. In brief, the thickness of the ONL from 3 to 5 consecutive sections per eye was measured. All sections were through the optic nerve in the ventral-dorsal axis of mice at 24 M of age. ONL thickness was measured 3 times per section at 4 inferior and 4 superior position spaced 500 µm apart. An average was generated for each section and for each retina. The measurements of the ONL were taken on DAPI-stained sections. Each group used 5 retinas per quantification.

## Phagocytosis assay

Phagocytosis assay was performed as previously described[31]. In brief, per RPE flat mount, 10 areas of 40,000 $\mu m^2$ within a 1.5 mm radius from the center were selected randomly to quantify the number of RHODOPSIN positive dots per RPE cell. Images for quantification were acquired at 20X. RPE cell boundaries were detected with anti-ZO1 antibody. Quantification was performed using IMARIS imaging processor by selecting a dot diameter > 2 µm to count dots and by counting the number of RPE cells per imaged field. The average dot number per RPE cell for a given RPE flat mount was obtained by averaging the results of the 10 fields. This number was then used to generate the average of the biological replicates, which was 6 mice for each group. RPE whole mounts were collected at 8am and 11am to evaluate the digestion of POSs by RPE cells over time.

### Transmission electron microscopy (EM)

Transmission Electron Microscopy (TEM) was performed as described[52]. In brief, mouse eyes were enucleated and fixed in 2.5% glutaraldehyde in 0.1 M sodium cacodylate buffer (pH 7.2) for 20 min at RT. Then, cornea and lens was removed and eyecups were fixed overnight at 4° C in the same fixative. Eyecups were washed three times with 0.1 M sodium cacodylate buffer and postfixed in 1% osmium tetroxide/ 0.1 M cacodylate buffer, dehydrated through an ethanol gradient to 100%, and embedded in epoxy resin. Semi-thin Sect. (1 µm) and ultrathin Sect. (70 nm) were cut with an ultramicrotome (Leica Reichart-Jung; Leica Microsystems) and stained with toluidine blue or 2% uranyl acetate and 4% lead citrate respectively. Semi-thin sections were visualized with a Leica DM6 Thunder microscope and ultrathin sections were visualized with a transmission electron microscope (Philips CM-10; Philips, Eindhoven, The Netherlands).

### VEGFA ELISA

A mouse VEGFA ELISA kit (Invitrogen, Cat#: EMVEGFACL) was used to quantify VEGFA levels in RPE/Choroid and retinal protein extract. Enucleated eyes were freshly dissected by removing cornea, lens and neural retina. For each biological sample, 1 RPE/choroid or 1 retina was homogenized in 100 µL lysis buffer followed by sonication. Analysis was performed according to the manufacturer's instructions. For each group, 4–6 retinas and the corresponding RPE/choroid tissues were collected.

### Quantitative Western blot analysis

All Western blot quantifications used 5–6 biological samples with each sample consisting of one retina or RPE. Protein extraction was performed as previously described[31]. In brief, enucleated eyes were dissected in cold PBS buffer. Dissected retinas (or RPE/Choroid) were immediately transferred into RIPA buffer (Thermo Scientific, Cat. #: 89900) with protease & phosphatase inhibitors (Thermo Scientific; Cat. #: 1861281) and homogenized by sonication. After 10 min centrifugation at 4 °C at 13,000 RPM, protein extracts were transferred into a fresh tube and protein concentration was quantified with the Bio-Rad Protein Assay (Cat. #: 500 – 0113,0114,0115). Each lane was loaded with 10 µg of total protein for quantification. The following primary antibodies were used: rabbit anti-PKM2 (1:1000; Cell Signaling Technology, Cat#4053), rabbit anti-HK2 (1:1000; Cell Signaling Technology, Cat#2867), rabbit anti-Elastin (1:1000; Elastin Products Company, Cat#PR387), rabbit anti-laminin (1:1000; Abcam, Cat#ab11575), rabbit anti-pS6 (Ser240/244) (1:1000; Cell Signaling Technology, Cat#5364), mouse anti-β-actin (1:1,000, Cell Signaling Technology, Cat#3700), goat anti-Apolipoprotein E (1:1,000, Millipore, Cat#178479), rabbit anti-HTRA1 (1:1000, Proteintech, Cat#55011-1-AP) and rabbit anti-complement factor H (1:1000; Antibodies Online Cat# ABIN3023097). β-actin was used to normalize sample variations. All controls used littermates to assess percentage changes. Protein detection used fluorescently labeled secondary antibodies (1:10,000) from Licor in combination with the Odyssey system. Quantification was performed with the Image Studio software. This combination of tools allows for optimal linear quantification, independent of any post-acquisition image modifications for visualization purposes.

### Statistical analysis

Two-tailed multiple t-test was used to assess statistically significant differences. Significance levels: $^{*}p<0.05$; $^{**}p<0.01$; $^{***}p<0.001$; $^{****}p<0.0001$. All bar graphs indicate mean and error bars represent the S.E.M. Fundus analysis bar graphs show the percentage of mice that developed the retinal pathologies described, while error bars represent margin of errors calculated with 90% confidence.

## Data availability

A synthesis of all experimental data related to this paper are available in the main text. All raw data from this study are available from the corresponding author upon reasonable request.

Received: 8 August 2024; Accepted: 31 March 2025
Published online: 10 April 2025

## References

1. Janciauskiene, S. M. et al. The discovery of alpha1-antitrypsin and its role in health and disease. *Respir. Med.* **105**, 1129–1139. https://doi.org/10.1016/j.rmed.2011.02.002 (2011).
2. Seixas, S. & Marques, P. I. Known mutations at the cause of alpha-1 antitrypsin deficiency an updated overview of SERPINA1 variation spectrum. *Appl. Clin. Genet.* **14**, 173–194. https://doi.org/10.2147/TACG.S257511 (2021).
3. Janciauskiene, S. et al. The multifaceted effects of alpha1-antitrypsin on neutrophil functions. *Front. Pharmacol.* **9**, 341. https://doi.org/10.3389/fphar.2018.00341 (2018).
4. Feitosa, P. H. Diagnosis and augmentation therapy for alpha-1 antitrypsin deficiency: Current knowledge and future potential. *Drugs Context.* **12** https://doi.org/10.7573/dic.2023-3-1 (2023).
5. Park, S. S. et al. Therapeutic potential of alpha-1 antitrypsin in type 1 and type 2 diabetes mellitus. *Med. (Kaunas).* **57** https://doi.org/10.3390/medicina57040397 (2021).
6. Collins, C. B. et al. Alpha-1-antitrypsin therapy ameliorates acute colitis and chronic murine ileitis. *Inflamm. Bowel Dis.* **19**, 1964–1973. https://doi.org/10.1097/MIB.0b013e31829292aa (2013).
7. Grimstein, C. et al. Alpha-1 antitrypsin protein and gene therapies decrease autoimmunity and delay arthritis development in mouse model. *J. Transl. Med.* **9** https://doi.org/10.1186/1479-5876-9-21 (2011).
8. Zhou, T. et al. Alpha-1 antitrypsin attenuates M1 microglia-mediated neuroinflammation in retinal degeneration. *Front. Immunol.* **9**, 1202. https://doi.org/10.3389/fimmu.2018.01202 (2018).
9. Moshirfar, M., Kelkar, N., Ronquillo, Y. C. & Hoopes, P. C. Assessing patients with alpha-1 antitrypsin deficiency for corneal refractive surgery: A review and clinical experience. *J. Clin. Med.* **11** https://doi.org/10.3390/jcm11144175 (2022).
10. Gorman, B. R. et al. Distinctive cross-ancestry genetic architecture for age-related macular degeneration. *medRxiv* https://doi.org/10.1101/2022.08.16.22278855 (2022).

11. Curcio, C. A. & Johnson, M. in *Retina Fith Edition* Vol. 1. 465–481 (Elsevier Inc., 2012).
12. Bhutto, I. & Lutty, G. Understanding age-related macular degeneration (AMD): Relationships between the photoreceptor/retinal pigment epithelium/bruch's membrane/choriocapillaris complex. *Mol. Aspects Med.* **33**, 295–317. https://doi.org/10.1016/j.mam.2012.04.005 (2012).
13. Garcia-Onrubia, L. et al. Matrix metalloproteinases in age-related macular degeneration (AMD). *Int. J. Mol. Sci.* **21** https://doi.org/10.3390/ijms21165934 (2020).
14. Neale, B. M. et al. Genome-wide association study of advanced age-related macular degeneration identifies a role of the hepatic lipase gene (LIPC). *Proc. Natl. Acad. Sci. U. S. A.* **107**, 7395–7400. https://doi.org/10.1073/pnas.0912019107 (2010).
15. Seddon, J. M., Reynolds, R. & Rosner, B. Associations of smoking, body mass index, dietary Lutein, and the LIPC gene variant rs10468017 with advanced age-related macular degeneration. *Mol. Vis.* **16**, 2412–2424 (2010).
16. Frochaux, V., Hildebrand, D., Talke, A., Linscheid, M. W. & Schluter, H. Alpha-1-antitrypsin: A novel human high temperature requirement protease A1 (HTRA1) substrate in human placental tissue. *PLoS One* **9**, e109483. https://doi.org/10.1371/journal.pone.0109483 (2014).
17. Yang, Z. et al. A variant of the HTRA1 gene increases susceptibility to age-related macular degeneration. *Science* **314**, 992–993. https://doi.org/10.1126/science.1133811 (2006).
18. Williams, B. L. et al. Chromosome 10q26-driven age-related macular degeneration is associated with reduced levels of HTRA1 in human retinal pigment epithelium. *Proc. Natl. Acad. Sci. U. S. A.* **118** https://doi.org/10.1073/pnas.2103617118 (2021).
19. Vierkotten, S., Muether, P. S. & Fauser, S. Overexpression of HTRA1 leads to ultrastructural changes in the elastic layer of Bruch's membrane via cleavage of extracellular matrix components. *PLoS One* **6**, e22959. https://doi.org/10.1371/journal.pone.0022959 (2011).
20. Nakayama, M. et al. Overexpression of HtrA1 and exposure to mainstream cigarette smoke leads to choroidal neovascularization and subretinal deposits in aged mice. *Invest. Ophthalmol. Vis. Sci.* **55**, 6514–6523. https://doi.org/10.1167/iovs.14-14453 (2014).
21. Navneet, S., Brandon, C., Simpson, K. & Rohrer, B. Exploring the therapeutic potential of elastase inhibition in age-related macular degeneration in mouse and human. *Cells* **12**. https://doi.org/10.3390/cells12091308 (2023).
22. Jones, A. et al. Increased expression of multifunctional serine protease, HTRA1, in retinal pigment epithelium induces polypoidal choroidal vasculopathy in mice. *Proc. Natl. Acad. Sci. U. S. A.* **108**, 14578–14583. https://doi.org/10.1073/pnas.1102853108 (2011).
23. Bellacen, K., Kalay, N., Ozeri, E., Shahaf, G. & Lewis, E. C. Revascularization of pancreatic islet allografts is enhanced by alpha-1-antitrypsin under anti-inflammatory conditions. *Cell. Transpl.* **22**, 2119–2133. https://doi.org/10.3727/096368912X657701 (2013).
24. Petrache, I. et al. A novel antiapoptotic role for alpha1-antitrypsin in the prevention of pulmonary emphysema. *Am. J. Respir. Crit. Care Med.* **173**, 1222–1228. https://doi.org/10.1164/rccm.200512-1842OC (2006).
25. Zelvyte, I., Stevens, T., Westin, U. & Janciauskiene, S. Alpha1-antitrypsin and its C-terminal fragment attenuate effects of degranulated neutrophil-conditioned medium on lung cancer HCC cells, in vitro. *Cancer Cell Int.* **4**, 7. https://doi.org/10.1186/1475-2867-4-7 (2004).
26. Kurtagic, E., Jedrychowski, M. P. & Nugent, M. A. Neutrophil elastase cleaves VEGF to generate a VEGF fragment with altered activity. *Am. J. Physiol. Lung Cell. Mol. Physiol.* **296**, L534–546. https://doi.org/10.1152/ajplung.90505.2008 (2009).
27. Borel, F. et al. Editing out five Serpina1 paralogs to create a mouse model of genetic emphysema. *Proc. Natl. Acad. Sci. U. S. A.* **115**, 2788–2793. https://doi.org/10.1073/pnas.1713689115 (2018).
28. Xu, H., Chen, M., Manivannan, A., Lois, N. & Forrester, J. V. Age-dependent accumulation of Lipofuscin in perivascular and subretinal microglia in experimental mice. *Aging Cell.* **7**, 58–68. https://doi.org/10.1111/j.1474-9726.2007.00351.x (2008).
29. Dorgau, B. et al. Laminin gamma3 plays an important role in retinal lamination, photoreceptor organisation and ganglion cell differentiation. *Cell. Death Dis.* **9**, 615. https://doi.org/10.1038/s41419-018-0648-0 (2018).
30. Hermenean, A. et al. Changes in retinal structure and ultrastructure in the aged mice correlate with differences in the expression of selected retinal MiRNAs. *Front. Pharmacol.* **11**, 593514. https://doi.org/10.3389/fphar.2020.593514 (2020).
31. Cheng, S. Y. et al. Altered photoreceptor metabolism in mouse causes late stage age-related macular degeneration-like pathologies. *Proc. Natl. Acad. Sci. U. S. A.* **117**, 13094–13104. https://doi.org/10.1073/pnas.2000339117 (2020).
32. Punzo, C., Kornacker, K. & Cepko, C. L. Stimulation of the Insulin/mTOR pathway delays cone death in a mouse model of retinitis pigmentosa. *Nat. Neurosci.* **12**, 44–52. https://doi.org/10.1038/nn.2234 (2009).
33. Venkatesh, A. et al. Activated mTORC1 promotes long-term cone survival in retinitis pigmentosa mice. *J. Clin. Invest.* **125**, 1446–1458. https://doi.org/10.1172/JCI79766 (2015).
34. Curcio, C. A. Soft drusen in age-related macular degeneration: Biology and targeting via the oil spill strategies. *Invest. Ophthalmol. Vis. Sci.* **59**, AMD160–AMD181. https://doi.org/10.1167/iovs.18-24882 (2018).
35. Saint-Geniez, M., Kurihara, T., Sekiyama, E.. Maldonado, A. E. & D'Amore, P. A. An essential role for RPE-derived soluble VEGF in the maintenance of the choriocapillaris. *Proc. Natl. Acad. Sci. U. S. A.* **106**, 18751–18756. https://doi.org/10.1073/pnas.0905010106 (2009).
36. Amadio, M., Govoni, S. & Pascale, A. Targeting VEGF in eye neovascularization: What's new? A comprehensive review on current therapies and oligonucleotide-based interventions under development. *Pharmacol. Res.* **103**, 253–269. https://doi.org/10.1016/j.phrs.2015.11.027 (2016).
37. Ortiz, G., Salica, J. P., Chuluyan, E. H. & Gallo, J. E. Diabetic retinopathy: Could the alpha-1 antitrypsin be a therapeutic option? *Biol. Res.* **47**, 58. https://doi.org/10.1186/0717-6287-47-58 (2014).
38. Kueppers, F. The expanding scope of alpha 1 antitrypsin deficiency. *Mayo Clin. Proc. Innov. Qual. Outcomes* **8**, 58–61. https://doi.org/10.1016/j.mayocpiqo.2023.12.001 (2024).
39. Fritsche, L. G. et al. Age-related macular degeneration: Genetics and biology coming together. *Annu. Rev. Genom. Hum. Genet.* **15**, 151–171. https://doi.org/10.1146/annurev-genom-090413-025610 (2014).
40. Fritsche, L. G. et al. A large genome-wide association study of age-related macular degeneration highlights contributions of rare and common variants. *Nat. Genet.* **48**, 134–143. https://doi.org/10.1038/ng.3448 (2016).
41. Velilla, S. et al. Smoking and age-related macular degeneration: Review and update. *J. Ophthalmol.* **2013**, 895147. https://doi.org/10.1155/2013/895147 (2013).
42. Seddon, J. M., Willett, W. C., Speizer, F. E. & Hankinson, S. E. A prospective study of cigarette smoking and age-related macular degeneration in women. *JAMA* **276**, 1141–1146 (1996).
43. Hubbard, R. C. et al. Oxidants spontaneously released by alveolar macrophages of cigarette smokers can inactivate the active site of alpha 1-antitrypsin, rendering it ineffective as an inhibitor of neutrophil elastase. *J. Clin. Invest.* **80**, 1289–1295. https://doi.org/10.1172/JCI113204 (1987).
44. Fujihara, M., Nagai, N., Sussan, T. E., Biswal, S. & Handa, J. T. Chronic cigarette smoke causes oxidative damage and apoptosis to retinal pigmented epithelial cells in mice. *PLoS One* **3**, e3119. https://doi.org/10.1371/journal.pone.0003119 (2008).
45. Geerlings, M. J., de Jong, E. K. & Den Hollander, A. I. The complement system in age-related macular degeneration: A review of rare genetic variants and implications for personalized treatment. *Mol. Immunol.* **84**, 65–76. https://doi.org/10.1016/j.molimm.2016.11.016 (2017).
46. Mattapallil, M. J. et al. The Rd8 mutation of the Crb1 gene is present in vendor lines of C57BL/6 N mice and embryonic stem cells, and confounds ocular induced mutant phenotypes. *Invest. Ophthalmol. Vis. Sci.* **53**, 2921–2927. https://doi.org/10.1167/iovs.12-9662 (2012).
47. Seddon, J. M. et al. Histopathological insights into choroidal vascular loss in clinically documented cases of age-related macular degeneration. *JAMA Ophthalmol.* **134**, 1272–1280. https://doi.org/10.1001/jamaophthalmol.2016.3519 (2016).

48. Seddon, J. M., Sharma, S. & Adelman, R. A. Evaluation of the clinical age-related maculopathy staging system. *Ophthalmology* **113**, 260–266. https://doi.org/10.1016/j.ophtha.2005.11.001 (2006).
49. Venkatesh, A., Ma, S., Langellotto, F., Gao, G. & Punzo, C. Retinal gene delivery by rAAV and DNA electroporation. *Curr. Protoc. Microbiol.* **28**, 14D. https://doi.org/10.1002/9780471729259.mc14d04s28 (2013).
50. Cheng, S. Y. et al. Low-dose rAAV-mediated inhibition of VEGF can treat neovascular pathologies without inducing retinal vasculitis. *Hum. Gene Ther.* https://doi.org/10.1089/hum.2021.132 (2021).
51. Petit, L. et al. Aerobic glycolysis is essential for normal rod function and controls secondary cone death in retinitis pigmentosa. *Cell. Rep.* **23**, 2629–2642. https://doi.org/10.1016/j.celrep.2018.04.111 (2018).
52. Ma, S. et al. Loss of mTOR signaling affects cone function, cone structure and expression of cone specific proteins without affecting cone survival. *Exp. Eye Res.* **135**, 1–13. https://doi.org/10.1016/j.exer.2015.04.006 (2015).

## Acknowledgements

This work was supported by a BrightFocus Foundation Grant M2020016 and a NIH Grant EY032461 to C.P., and by a Macular Degeneration Center of Excellence Fund, University of Massachusetts Chan Medical School, Department of Ophthalmology and Visual Sciences and a NIH Grant EY028602 to J.M.S.

## Author contributions

S.-Y.C. and C.P. conceived and performed experiments, interpreted data, and wrote the manuscript. D.G., I.S., A.C., S.K. performed experiments. J.M.S. provided human tissue samples. T.K. provided reagents. C.M. conceived initial experiments with C.P. All authors have read and agreed to the published version of the manuscript.

## Declarations

## Competing interests

The authors declare no competing interests.

## Additional information

**Supplementary Information** The online version contains supplementary material available at https://doi.org/10.1038/s41598-025-96570-x.

**Correspondence** and requests for materials should be addressed to C.P.

**Reprints and permissions information** is available at www.nature.com/reprints.

**Publisher's note** Springer Nature remains neutral with regard to jurisdictional claims in published maps and institutional affiliations.